Sirte University Scientific Journal (Applied Sciences) *Vol.8(1),07–20 June 2018*

The Effect of Current Density, Time and Anodizing Temperature on The Local Burning of Anodic Alumina Films

Ali K. M. Al-zenati
e-mail: alikmz@yahoo.co.uk

Department of Mechanical, Faculty of Engineering, Sirte University

Abstract

The local burning phenomenon on the surface of the anodic alumina films is studied under wide range of current densities, anodizing times and anodizing temperature. The growth of nodules occurs at low anodizing temperature (0 ^{0}C) and at relatively high current density (10-40 mA/cm^2). However, the local burning does not obtain at low current density i.e. 5 even at 0 ^{0}C. Moreover nodules formation is not existed on the surface of the anodic alumina films fabricated under the same previous anodizing conditions (5-40 mA/cm^2) but at high anodizing temperature (20 ^{0}C). In fact, the increment of current density, voltage or electric field increases the local heat. Dissipation of local heat plays big role to prevent local burning rather than reduction of anodizing temperature. Therefore heat transfer is more important than decreased temperature of the electrolyte only which is enhanced the local burning. No obvious effect of anodizing time on occurrence of local burning because of the initial growth of nodules forms at the first seconds of anodizing time. The initial behavior of the voltage-time response and the $\Delta V/\Delta t$-time transient is a good indicator for nodules growth.

Keywords: *Anodizing, Anodic alumina film, Local Burning.*

1. Introduction

Anodic porous alumina films have been widely investigated[1-6] for many applications: such as wear resistance[7,8] and nano-technology i.e. anti reflection structures[9,10], reflectors[11], sensors[12], diodes[13], memory devices[14], optical devices[15,16], microlens arrays[17,18], nano containers[19], nano-templates[20,21], plasmonic devices[22], resist masks[23,24], photonic crystals[25–27], catalyst supports[28], evaporation masks[29].

Aluminium under specific anodizing conditions is subjected to burning phenomenon. It is caused by high local temperature[30-33] which arises from very high local current density. The burning appears as thicker degraded oxide which has different colours according to electrolyte types e.g. whitish spot for films formed in sulphuric or phosphoric acid electrolytes. However, it takes a black or brown colour when anodizing in organic electrolytes, such as oxalic and malonic

acid[30,31,34]. The formation of burning during anodizing process can be enhanced by certain factors i.e. low anodizing temperature, high current densities, low acid concentration, or the addition of sulphate salts to the sulphuric acid electrolyte. Voltage-time and ΔV/Δt-time responses show four steps of anodic film formation as revealed in figure (1-1). Step (1) refers to initial formation of anodic film; step (2) starting of nanopores initiation at the beginning of this step which extends between the maximum value of ΔV/Δt to a value of zero; step (3) the stage extending between zero value of ΔV/Δt to negative values followed by rising up to form a valley. The valley shape being effected by anodizing conditions such as, increasing current density, reducing acid concentration and decreasing temperature lead to change in the shape of valley forming nodules; step (4), it starts when the value of ΔV/Δt is zero and the voltage value becomes steady[35]. Many efforts revealed that the initiation of burning is associated with local phenomenon of the developing heat during aluminium anodizing.

The balance between the generated heat that produces during the anodizing process and the heat removed plays big role in the initiation of burning[30-33]. Local heat generation is related to Joule heating effects, which occur as result of the ionic current passing across the highly resistive oxide layer. Local heat increases with rise of the anodizing current density or voltage. Removal of local heat during anodizing is mainly dependent upon the conductivity of the aluminium substrate and the electrolyte convection, and hence the electrolyte agitation system.

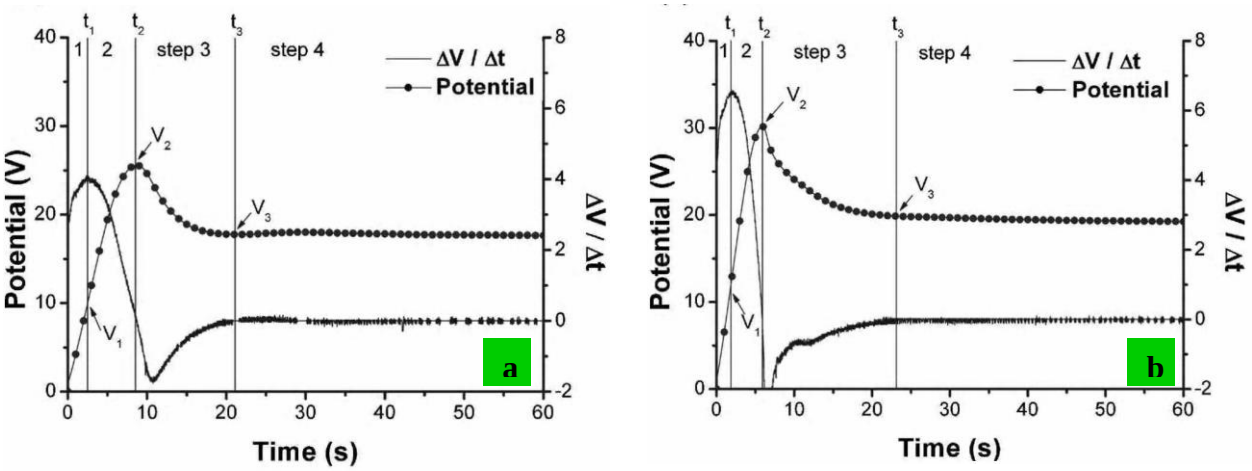

Figure 1. Potential-time responses and its differentiated curves for an Al1050 specimen anodized in a 15 wt % sulphuric acid at 15 mA/cm^2 and 293 k; the different times of t_1, t_2 and t_3 correspond to different potentials V_1, V_2 and V_3: current density of (a) 12 mA/cm^2, (b) 18 mA/cm^2 [37].

Burning initiates on thinner electrodes rather than thicker electrodes because heat conduction and distribution of local heat away from the aluminium/film interface is restricted to a small volume of aluminium substrate[30,36]. Aggravation of burning increases in hard anodizing rather than

conventional anodizing because of controlling factor of triggering of burning is the heat transfer instead of the heat alone[30,32,33]. Measurements[31-33] showed a sudden increase of local temperature in the burning area and the surrounding region. Moreover, high local current density is reported on high local thicknesses of the film in the burning area[31-33]. The flaws in the oxide film during the burning act as conductive paths leading to highly concentrated current. The formation of burning occurs in the stage of low fluctuations and deflections in the initial decrease of anodizing voltage which corresponds to a rise in local temperatures in the burning area coinciding with reductions in temperature in the non-burning area. The oxide nodules are made of two regions; the upper region is a porous tube-like microstructure covered by a thin porous layer, whereas the lower region has a microstructure similar to the rest of the alumina oxide in the non-burning area.

2. Experimental Work

Specimens made of high purity aluminium (99.99 %) sheet 0.3 mm thickness were prepared and anodized as follows:

Process of preparation and cleaning of specimens: The aluminium sheet was cut into pieces of dimensions 1.5 x 2.5 cm^2 then the specimens were degreased in ethanol.

Process of electro-polishing: This process was achieved in 1000 ml glass beaker, containing a mixture of perchloric-ethanol electrolyte (1:4 vol.) was stirred magnetically at constant voltage of 20 V for 180 s below 10 C˚ to reduce the surface roughness. Each specimen was connected to the positive terminal of a direct current (d.c.) power supply, working as an anode, whereas a cylindrical plate of high purity aluminium foil acts as a cathode. Then the specimens were cleaned in ethanol and deionized water respectively and then drying by a cool air stream. Finally the specimen edges were covered by insulating material (lacquer 45) in order to define the working area (1 x 2 cm^2).

Process of anodizing: Anodizing cell consists of a 1000 ml glass beaker, a paddle stirrer and a thermometer. Electro-polished specimens were individually anodized under selected constant current densities 5, 10 and 20 mA/cm^2 for constant anodizing time of 5400 s and at 40 mA/cm^2 for different anodizing times for 1000, 3000, 4000 and 5400 s in 24.5 wt % sulphuric acid at 0 and 20 C˚. The specimen (1 x 2 cm^2) was connected to the positive terminal of a d.c. power, working as an anode in two-electrode, glass cell with a cylindrical sheet of high purity aluminium foil (8 x 22 cm^2) was connected to the negative terminal of power supply, functioning as a cathode. Lastly, the resultant anodic films were rinsed with deionized water and dried under a cool air stream for investigation
of the surface morphology and the voltage-time response.

Specimen examination

Optical interferometry technique

It is a technique based on electromagnetic waves. It is rely on interference of two or more superimposed reflections of the input laser beam in order to extract information. Instrument

utilized MapVue^{TM} mapping and analysis software to provide surface information. It is an important investigative technique in many fields such as astronomy, optical metrology, spectroscopy, quantum mechanics, nuclear, particle physics, plasma physics, biomolecular interactions, surface profiling, microfluidics, mechanical stress/strain measurement, velocimetry, and optometry. Specimen can be examined by focusing the light beam on its surface.

Ultra high resolution field emission scanning electron microscopy (FESEM)

FESEM employed an Ultra 55 (GEMINI® technology) microscope. The microscope gives high resolution for both secondary electrons (SE) to image surface information and backscattering secondary electrons (BSE) to supply compositional information. The angle-selective backscattered electron (EsB) features an integrated filtering grid to enhance quality of image and no additional adjustments requires. Moreover the EsB detector has less sensitivity to edge contrast and charging influences, which provides good precise imaging.

3. Results

Voltage-time behavior at 0 ^{0}C

The voltage-time transient of anodizing at 5 mA/cm^2 for 5400 s, reveals that the voltage rises linearly with increase in anodizing time to roughly 22.5 V in the first 17 s. The voltage then decreases to 16.6 V within 37 s, followed by a rise to 17.4 V as shown in figure (3-1-a).

The typical voltage-time response of a specimen anodized at 10 mA/cm^2 for 5400 s, is shown in figure (3-1-c). The voltage firstly increases linearly with time to approximately 27 V within 10 s. During the subsequent 25 s, the voltage then drops to about 20.2 V.

The voltage-time transient in figure (3-1-e) of film fabricated at 20 mA/cm^2 for 5400s. The anodizing voltage increases linearly up to 28.8 V within 5 s. After that the voltage increases 23.1 V within 23 s.

For a specimen anodized at 40 mA/cm^2 for 5400 s. From the commencement of the experiment, the voltage increases linearly with increase in time until a voltage reaches approximately 30.9 V within 3 s, followed by sharp reduction to 24.3 V as revealed in figure (3-1-g).

Voltage-time behavior at 20 ^{0}C

The voltage-time response for specimen anodized at 5 mA/cm^2 for 5400 s is revealed in figure (3-1-b). In the first 12 s, an initial linear increment of anodizing voltage to approximately 8.7 V, is followed by rapid reduction to 7.7 V during 20 s. It then increases to about 8.2 V until the end of the anodizing process.

The voltage-time transient is revealed in figure (3-1-d) for specimen anodized at10 mA/cm^2 for 5400 s. A surge of voltage to nearly12.6 V within 8 s, is followed by a steep decrease in voltage to reach a minimum value of about 10.8 V during a time of about 14 s. The voltage then rises slowly, reaching a steady value of 11.5 V at the termination of the experiment.

The voltage-time response for film formed at 20 mA/cm^2 for 5400s. Initially, the anodizing voltage surges to approximately 19.3 V in 5 s, followed by a steep decline to roughly 14.5 V. It then increases to roughly 15.8 V as seen in figure (3-1-f).

Figure (3-1-h) shows the voltage-time response for specimen anodized at 40 mA/cm^2 for 5400 s. At the beginning of the anodizing process, the voltage increases to approximately 22.5 V within 3 s, followed by a relatively a sharp reduction to a minimum value of around 18.1 V.

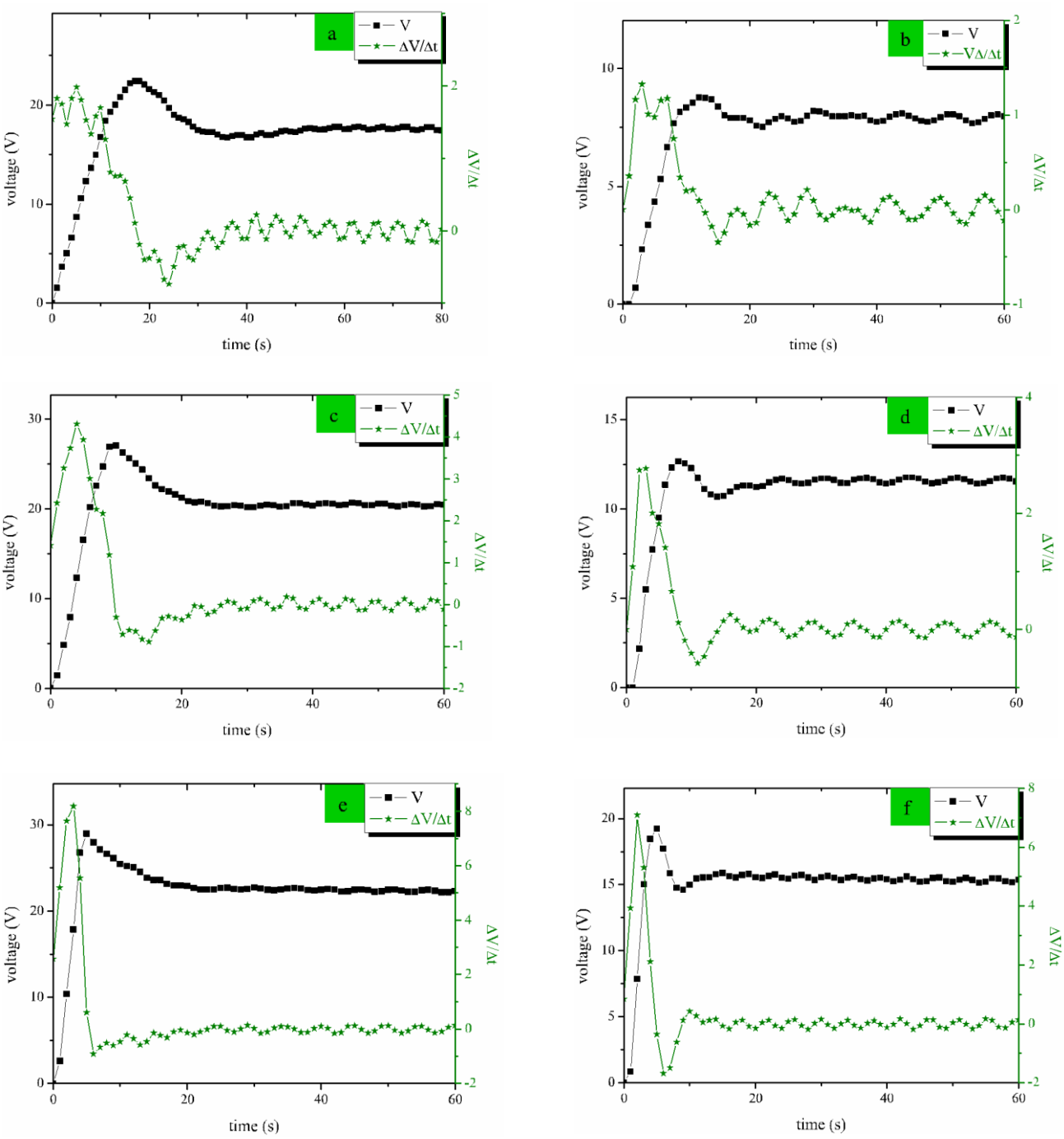

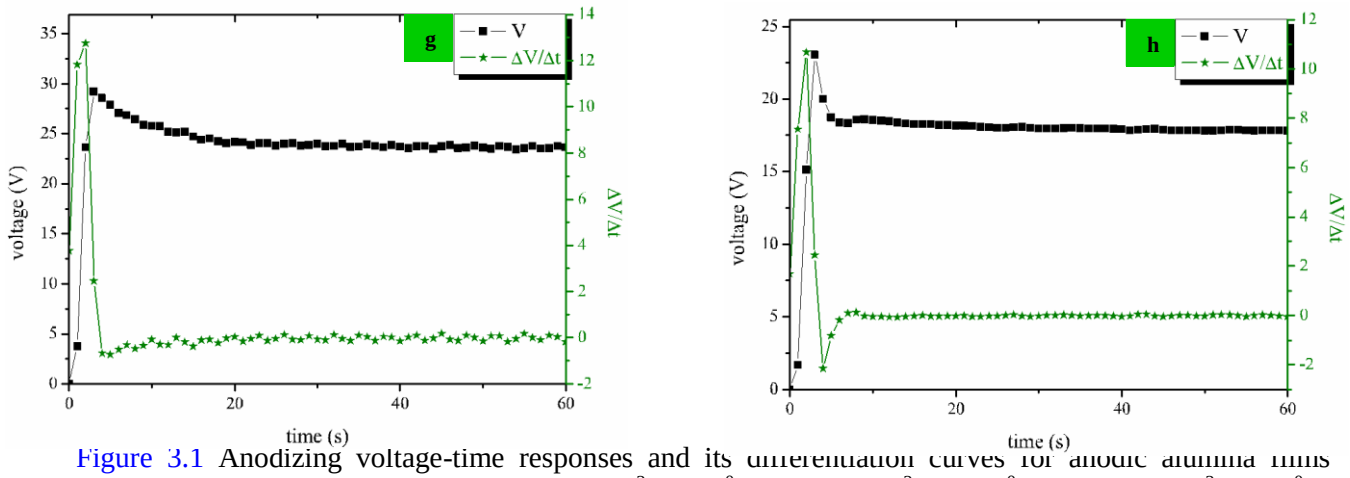

Figure 3.1 Anodizing voltage-time responses and its differentiation curves for anodic alumina films fabricated for 5400 s at; a- 5 mA/cm^2 and 0 ^{0}C, b-5 mA/cm^2 and 20 ^{0}C, c- 10 mA/cm^2 and 0 ^{0}C, d- 10 mA/cm^2 and 20 ^{0}C, e- 20 mA/cm^2 and 0 ^{0}C, f- 20 mA/cm^2 and 20 ^{0}C, g- 40 mA/cm^2 and 0 ^{0}C and h- 40 mA/cm^2 and 20 ^{0}C.

Nodules on the film surface

Table 1. Height and width of the nodules on the anodic alumina films.

Current densi mA/cm^2	Anodizing t (s)	Final anodizir voltage (v)	Height (µm)	Width (µm)	Ratio of nodule h to film thickness (	Figu No.
10	5400	19.7	6.6	26.83	22	3-2
20	5400	23.3	0.6	01.69	1.0	3-3
20	5400	23.3	4.0	20.20	6.0	3-4
40	1000	24.1	3.1	14.94	13	3-5
40	1000	24.1	3.4	16.14	14	3-6
40	5400	34.2	4.6	21.91	3.0	3-7

Nodules appear on surface of films formed on electropolished aluminium at 10, 20 and 40 mA/cm^2 at 0 ^{0}C. However, nodules were not presented on films grown at lower current density i.e. 5 mA/cm^2 at 0 ^{0}C or on films formed at the same current densities namely, 5, 10, 20 and 40 mA/cm^2 but at high temperature i.e. 20 ^{0}C.

In fact, nodules were observed on films formed at 40 mA/cm^2 in 24.5 wt % sulphuric acid for 1000, 3000, 4000 and 5400 s with respective final anodizing voltages of 24.1, 29.1,

29.7 and 34.2 V. For films fabricated at 10 and 20 mA/cm^2 for anodizing time for 5400 s, nodules were detected with final anodizing voltage 19.7 and 23.3 V respectively.

Figures of profile micrographs from optical interferometry technique provide the dimensions of the nodules for films formed at various current densities at 0 ˚C. Figure (3-2) shows the values of width and height are 26.83 and 6.61 µm respectively for nodules grown on films formed at 10 mA/cm^2 for 5400 s. The width of nodules formed on films fabricated at 20 mA/cm^2 for 5400 s extends over the range 1.69 to 20.20 µm, with a lowest height of 0.61 and a highest height of 4.00 µm, as shown in figures (3-3) and (3-4). For films fabricated at 40 mA/cm^2 for various times, namely 1000 and 5400 s, the width ranges from 3.10 to 4.60 µm, with heights in the range of 14.94 to 21.91 µm, as revealed in figures (3-5), (3-6) and (3-7). Table (3-1) shows the height and width of the nodules formed on the anodic alumina films with final anodizing voltage.
For films grown at 20 mA/cm^2 for 5400 s, only three nodules are evident as seen in figure (3-8). Five or six circles of cracking reveal to be evident between the top and the base of the nodule for anodic alumina film fabricated at 40 mA/cm^2 for 3000 s as shown in figure (3-9). For film formed at 40 mA/cm^2 for 4000 s, the distribution of the nodules is non-uniform as shown in figure (3-10). Figure (3-11) reveals the initial growth of nodules underneath the film surface.

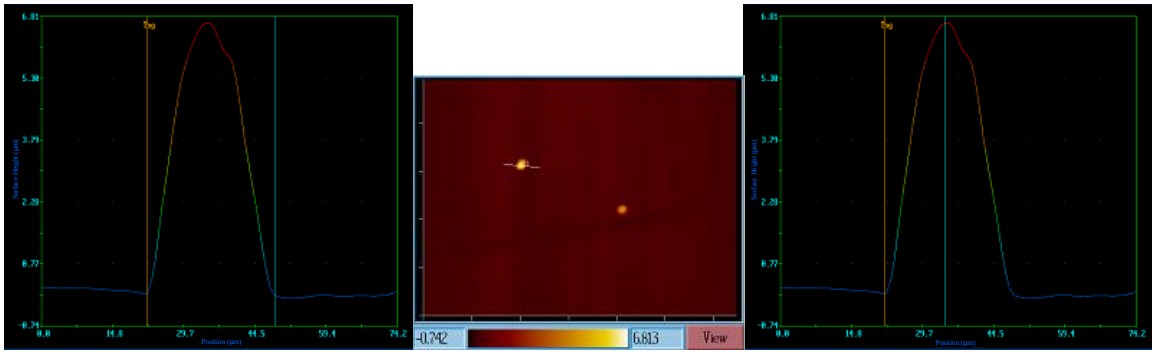

Figure 3-2. The measurements of height and width of nodules grown on the film fabricated at 10 mA/cm^2 for 5400 s at 0 ^{0}C.

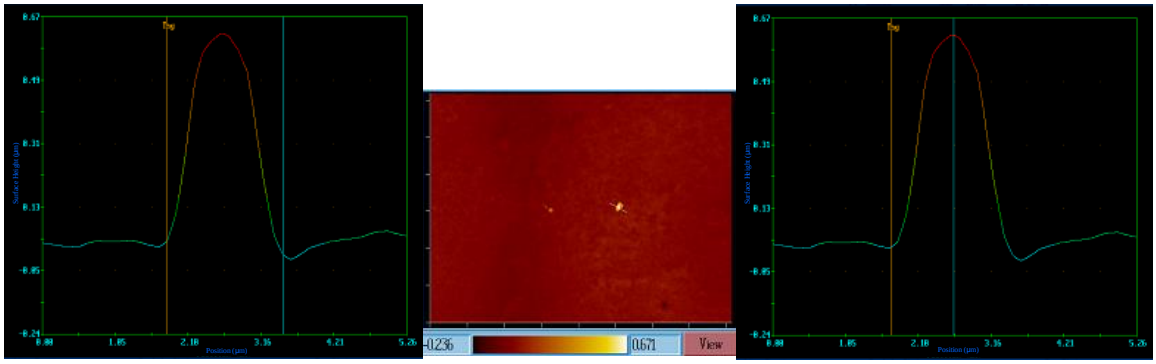

Figure 3-3. The measurements of height and width of nodules grown on the film fabricated at 20 mA/cm^2 for 5400 s at 0 ^{0}C.

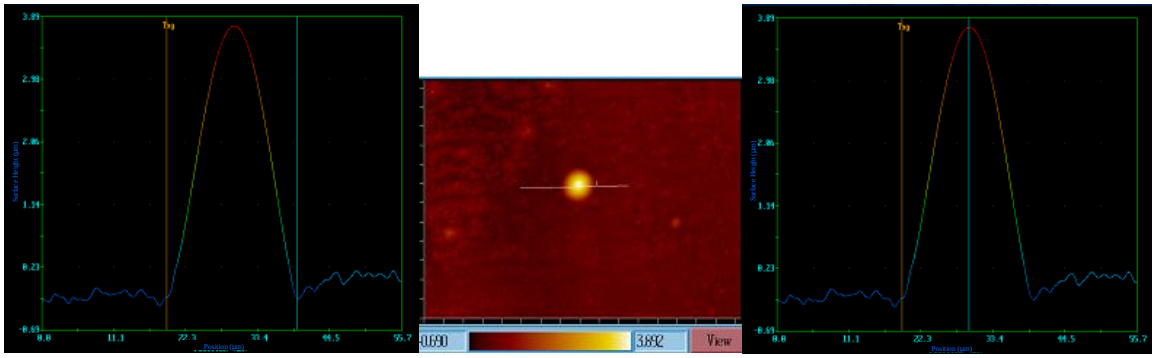

Figure 3-4. The measurements of height and width of nodules grown on the film fabricated at 20 mA/cm^2 for 5400 s at 0 ^{0}C.

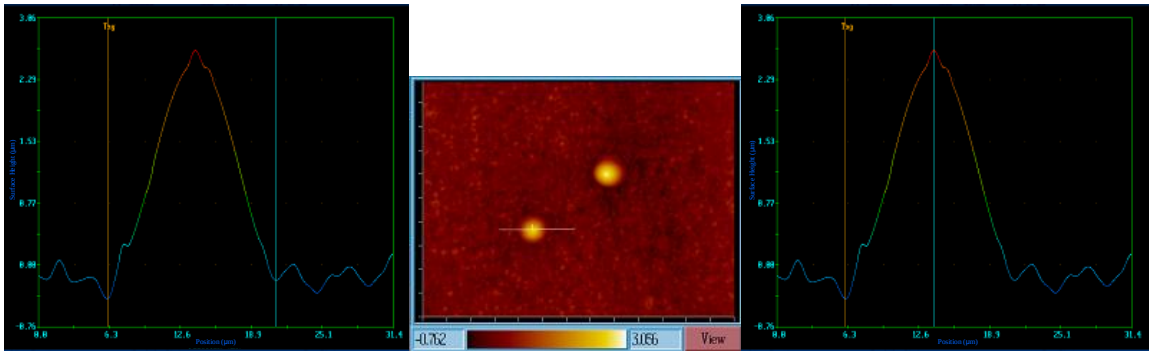

Figure 3-5. The measurements of height and width of nodules grown on the film fabricated at 40 mA/cm^2 for 1000 s at 0 ^{0}C.

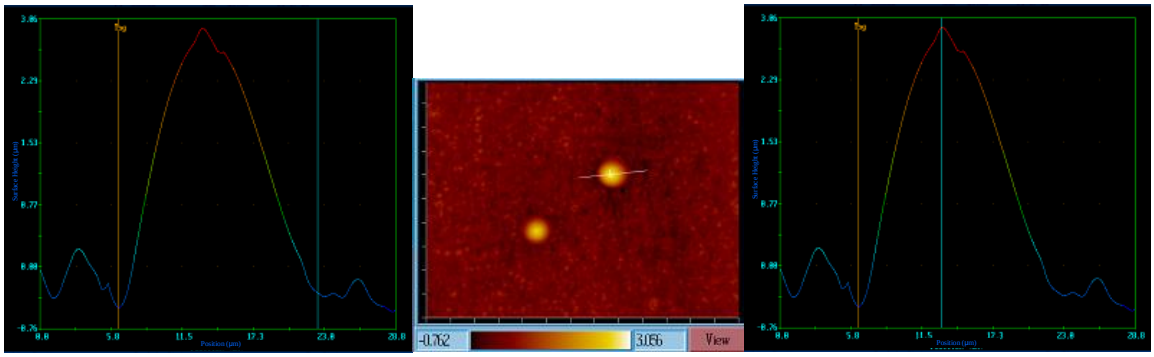

Figure 3-6. The measurements of height and width of nodules grown on the film fabricated at 40 mA/cm^2 for 1000 s at 0 ^{0}C.

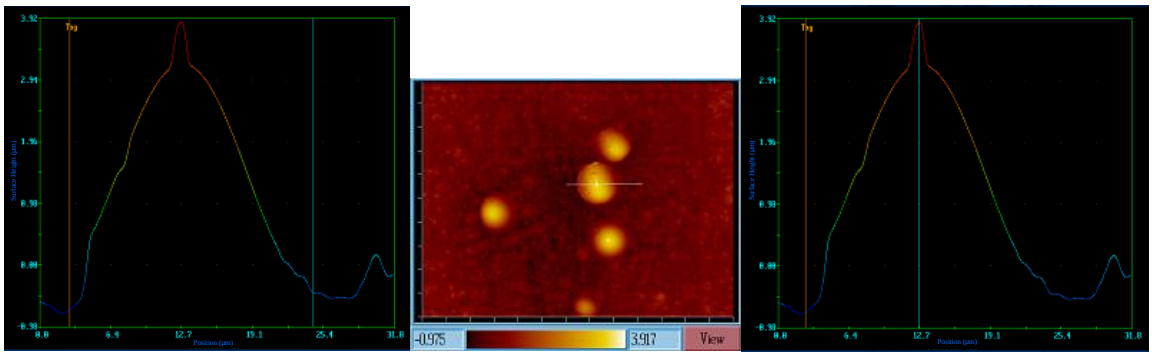

Figure 3-7. The measurements of height and width of nodules grown on the film fabricated at 40 mA/cm^2 for 5400 s at 0 ^{0}C.

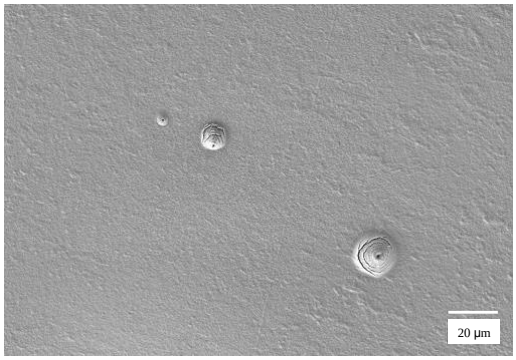

Figure 3-8. SEM micrographs of anodic alumina formed at 20 mA/cm^2 for 5400 s at 0 ^{0}C.

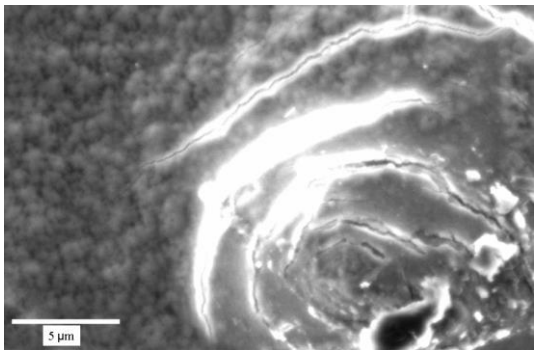

Figure 3-9. SEM micrographs of anodic alumina formed at 40 mA/cm^2 for 3000 s at 0 ^{0}C.

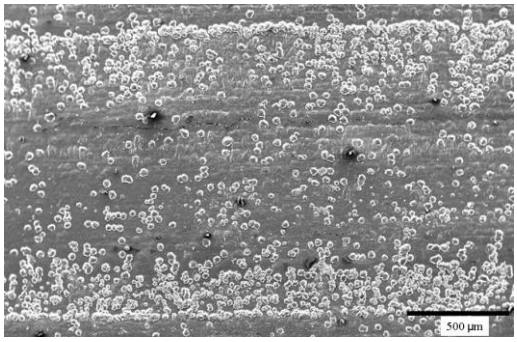

Figure 3-10. SEM micrographs of anodic alumina formed at 40 mA/cm^2 for 4000 s at 0 ^{0}C.

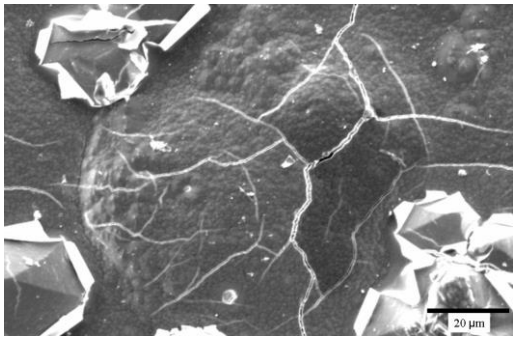

Figure 3-11. SEM micrographs of anodic alumina formed at 40 mA/cm^2 for 4000 s at 0 ^{0}C.

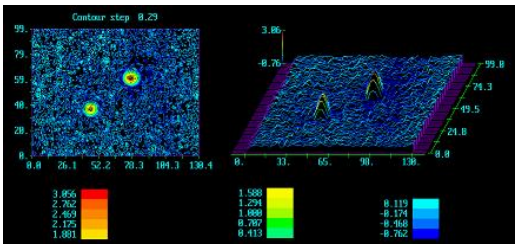

Figure 3-12. Interferometry micrographs of anodic alumina formed at 40 mA/cm^2 for 1000 s at 0 ^{0}C.

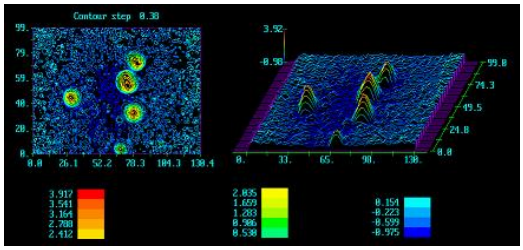

Figure 3-13. Interferometry micrographs of anodic alumina formed at 40 mA/cm^2 for 5400 s at 0 ^{0}C.

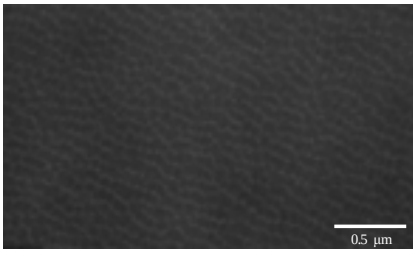

Figure 3-14. SEM micrographs of anodic alumina formed at 5 mA/cm^2 for 5400 s at 0 ^{0}C.

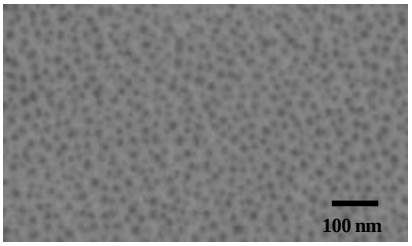

Figure 3-15. SEM micrographs of anodic alumina formed at 5 mA/cm^2 for 5400 s at 20 ^{0}C.

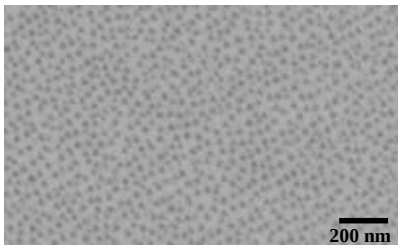

Figure 3-16. SEM micrographs of anodic alumina formed at 10 mA/cm^2 for 5400 s at 20 ^{0}C.

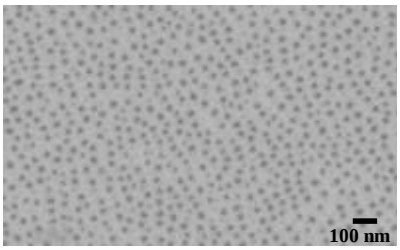

Figure 3-17. SEM micrographs of anodic alumina formed at 20 mA/cm^2 for 5400 s at 20 ^{0}C.

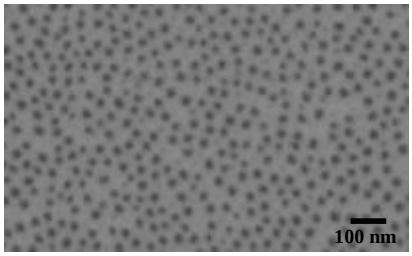

Figure 3-18. SEM micrographs of anodic alumina formed at 40 mA/cm^2 for 5400 s at 20 ^{0}C.

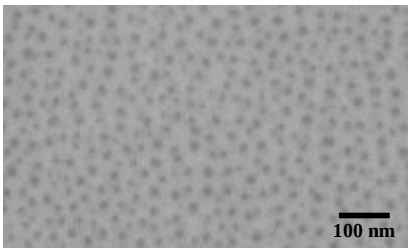

Figure 3-19. SEM micrographs of anodic alumina formed at 40 mA/cm^2 for 4000 s at 20 ^{0}C.

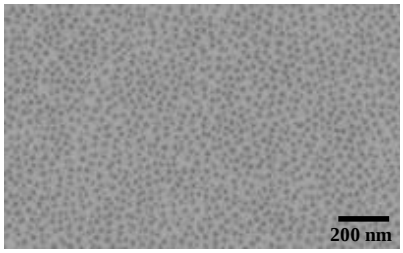

Figure 3-20. SEM micrographs of anodic alumina formed at 40 mA/cm^2 for 3000 s at 20 ^{0}C.

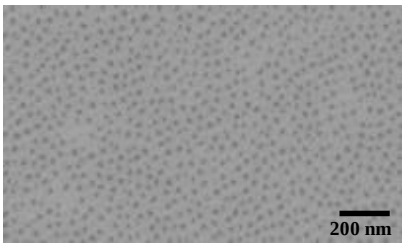

Figure 3-21. SEM micrographs of anodic alumina formed at 40 mA/cm^2 for 1000 s at 20 ^{0}C.

Moreover, the nodules are pyramid-like containing several faces, with approximately sharp or hemispherical tips, as seen in figure (3-11). A smooth thin layer of material is clear to be present to peel back from the sides of the nodules as in figure (3-11). Three-dimensional micrographs of anodic alumina films formed at 40 mA/cm^2 for 1000 and 5400 s at 0 ^{0}C can be seen in figures (3-12) and (3-13) respectively. SEM micrographs of anodic alumina films formed at 5 mA/cm^2 for 5400 s at 0 ^{0}C, and at 5, 10, 20 mA/cm^2 for 5400 s and 40 mA/cm^2 for 1000, 3000, 4000 and 5400 s but at 20 ^{0}C reveal no nodules appear as shown in figures (3-14) to (3-21).

4. Discussion

The hard films fabricated under 10, 20 and 40 mA/cm^2 contain nodules on their outer surfaces, contrary to films which are formed by conventional anodizing. The formation of nodules is associated with high local temperature that is due to catastrophic local flow of current on the anodizing aluminium surface[30-33]. The passage of ionic current across the highly resistive oxide film causes local heat. The increase of electric field, current density or voltage results in the rise of local heat. The heat transfer, unlike heat reduction alone, governs the burning, such that promoted cooling by a reduced temperature of the bulk electrolyte only enhances burning[30,32,33]. Dissipation of local heat is dependant on the conductivity of the aluminium and the convection of the electrolyte, and hence the agitation system should be utilized. The deflections and minor fluctuations in the initial reduction of the anodizing voltage are related to the formation of the nodule. This initial reduction of the anodizing voltage corresponds to the rise in local temperature in the burning area and reduction of temperature in non-burning area[38]. In the current study, the existence of nodules coincides with roughly similar features of the voltage-time response behaviour, namely the nodules grow when the anodizing voltage decreases slowly to the steady state region, which is approximately compatible with previous work of Tim el at[38]. The shape of the voltage-time transient in anodizing processes gives a more significant indicator of nodule formation rather than the value of the final anodizing voltage. The anodizing temperature is the most important factor which affects the shape of the voltage-time transient i.e. at high temperature, the minimum voltage lies significantly below the steady value characterizing by no nodule growth occurs although the value of the final anodizing voltage is high. In the

present results, nodules formation depends on the various types of the valleys in the differentiated curves as seen in figure (3-1), which agreement in previous study[37]. The nodule growth is related to change of the valley in the ΔV/Δt-time response, namely the ΔV/Δt after the valley "negative peak" increases to reach the steady value with small slope and without passing through the steady stage of the ΔV/Δt. In reality, the shape of voltage-time or ΔV/Δt-time provides a good evidence of the nodules existence with anodizing especially at high current density rather than at low current density.

5. Conclusion

The appearance of nodules is obvious on the surface of the anodic alumina films fabricated at 0 ^{0}C at wide range of current densities of 10 and 20 mA/cm^2 for 5400 s, and 40 mA/cm^2 for 1000, 3000, 4000 and 5400 s. However, for anodic alumina films formed at 5 mA/cm^2 at 0 ^{0}C for 5400 s, no nodules grow. The anodic alumina films grown under the same anodizing conditions, but at 20 ^{0}C, no nodules are present although the final anodizing voltage is relatively high. Anodizing time has no clear influence on the nodules formation. The growth of nodules is related to the shape of; the voltage-time transient and the ΔV/Δt-time transient. The voltage-time response i.e. the peak value of anodizing voltage decreases with low slope to a steady stage without passing through it. The ΔV/Δt-time transient, the value of the negative peak in ΔV/Δt is wide and increases to zero with no passing through the steady level. At specific current density, the temperature of anodizing governs the local burning instead of the final anodizing voltage.

References:

[1] X. Qina, J. Zhang, X. Menga, C. Denga, L. Zhang, G. Dingb, H. Zeng, X. Xu. Preparation and analysis of anodic aluminum oxide films. *J. Applied Surface Scien 328 (2015) 459–465.*

[2] R.K. Choudhary, P. Mishra,V. Kain, K. Singh, S.Kumar, J.K. Chakravart. Scratch behavior of aluminum anodized in oxalic acid. *J. Surface & Coatings Technology 283 (2015) 135–147.*

[3] M. Pashchanka, J. J. Schneider. Self-Ordering Regimes of Porous Anodic Alumina. *J. Phys. Chem., 120, (2016) 14590−14596.*

[4] Yi Li, Y. Qin, S. Jin, X. Hu, Z. Ling, Q. Liu, J Liao, C. Chen, Y. Shen, L. Jin. *J. Electrochimica Acta 178 (2015) 11–17.*

[5] J. Evertsson, N. A. Vinogradov, G. S. Harlow, F. Garla. S. R. Mckbbin, L. Rullik, W. Linpe, R. Felici, E. Lundgren. Self Organization of Porous Anodic Alumina Films. *RSC Advances, 34,(2018).*

[6] Z. B. Yang, J. C. Hu, K. Q. Li, S. Y. Zhang, Q. H. Fan, S. A. Liu. Advances of The Research Evolution on Aluminium. *Conference series: Materials Science and Engineering Vol.282(2018)10P.*

[7] V.R. Capelossi, M. Poelman, I. Recloux, R.P.B. Hermandes, H.G. de Melo, M.G. Olivier, Corrosion protection of clad 2024 aluminum alloy anodized in tartaric-sulfuric acid bath and protected with hybrid sol–gel coating, *Electrochim. Acta124 (2014) 6979.*

[8] T. Kikuchi, Y. Hara, M. Sakairi, T. Yonezawa, A. Yamauchi, H. Takahashi, Corrosion of Al–Sn–Bi alloys in alcohols at high temperatures. Part II: Effect of anodizing on corrosion, *Corr. Sci. 52 (2010) 2525–2534.*

[9] T. Yanagishita, M. Masui, N. Ikegawa, H. Masuda, Fabrication of polymer antire-flection structures by injection molding using ordered anodic porous alumina mold, *J. Vac. Sci. Technol. B 32 (2014) 021809.*

[10] T. Yanagishita, K. Nishio, H. Masuda, Anti-reflection structures on lenses by nanoimprinting using ordered anodic porous alumina, *Appl. Phys. Express 2 (2009) 022001.*

[11] G.D. Sulka, K. Hnida, Distributed Bragg reflector based on porous anodic alumina fabricated by pulse anodization, *Nanotechnology 23 (2012) 075303.*

[12] E. Kurowska, A. Brzózka, M. Jarosz, G.D. Sulka, M. Jaskuła, Silver nanowire array sensor for sensitive and rapid detection of H2O2, *Electrochim. Acta 104 (2013) 439–447.*

[13] S. Zhang, L. Wang, C. Xu, D. Li, L. Chen, D. Yang, Fabrication of NiNiO–Cu metal–insulator–metal tunnel diodes via anodic aluminum oxide templates, *ECS Solid State Lett. 2 (2013) Q1–Q4.*

[14] D. Liu, C. Zhang, G. Wang, Z. Shao, X. Zhu, N. Wang, H. Cheng, Nanoscale elec-trochemical metallization memories based on amorphous (La,Sr) MnO3using ultrathin porous alumina masks, *J. Phys. D: Appl. Phys. 47 (2014) 085108.*

[15] Q. Lin, B. Hua, S. Leung, X. Duan, Z. Fan, Efficient light absorption with integrated nanopillar/nanowell arrays for three-dimensional thin-film photovoltaic applications, *ACS Nano 7 (2013) 2725–2732.*

[16] T. Yanagishita, K. Nishio, H. Masuda, Fabrication of two-dimensional polymer photonic crystals by nanoimprinting using anodic porous alumina mold, *J. Vac. Sci. Technol. B 28 (2010) 398–400.*

[17] T. Kikuchi, Y. Wachi, T. Takahashi, M. Sakairi, R.O. Suzuki, Fabrication of a meniscus microlens array made of anodic alumina by laser irradiation and electrochemical techniques, *Electrochimica Acta 94 (2013) 269.*

[18] H. Jha, T. Kikuchi, M. Sakairi, H. Takahashi, Microfabrication of an Anodic Oxide Film by Anodizing Laser-textured Aluminum, *Journal of Micromechanics and Microengineering 17 (2007) 1949.*

[19] T. Kikuchi, Y. Akiyama, M. Ueda, M. Sakairi, H. Takahashi, Fabrication of a three-dimensional micro-manipulator by laser irradiation and electrochem-ical techniques and the effect of electrolytes on its performance, *Electrochim. Acta 52 (2007) 4480.*

[20] F. Keller, M.S. Hunter, D.L. Robinson, Structural Features of Oxide Coatings on Aluminum, *Journal of the Electrochemical Society 100 (1953) 411.*

[21] G.E. Thompson, R.C. Furneaux, G.C. Wood, J.A. Richardson, J.S. Gode, Nucleation and growth of porous anodic films on aluminium, *Nature 272 (1978) 433.*

[22] J. Wang, M. Singh, M. Tian, N. Kumar, B. Liu, C. Shi, J.K. Jain, N. Samarth, T.E. Mal-louk, M.H.W. Chan, Interplay between superconductivity and ferromagnetism in crystalline nanowires, *Nature Physics 6 (2010) 389.*

[23] J.E. Houser, K.R. Hebert, The role of viscous flow of oxide in the growth of self-ordered porous anodic alumina films, *Nature Materials 8 (2009) 415.*

[24] K.R. Hebert, S.P. Albu, I. Paramasivam, P. Schmuki, Morphological instability leading to formation of porous anodic oxide films, *Nature Materials 11 (2012) 162.*

[25] H. Masuda, M. Yamada, F. Matsumoto, S. Yokoyama, S. Mashiko, M. Nakao, K. Nishio, Lasing from two-dimensional photonic crystals using anodic porous alumina, *Advanced Materials 18 (2006) 213.*
[26] J. Choi, Y. Luo, R.B. Wehrspohn, R. Hillebrand, J. Schilling, U. Göele, Perfect two-dimensional porous alumina photonic crystals with duplex oxide layers, *Journal of Applied Physics 94 (2003) 4757.*
[27] Q. Lin, B. Hua, S.F. Leung, X. Duan, Z. Fan, Efficient Light Absorption with Integrated Nanopillar/Nanowell Arrays for Three-Dimensional Thin-Film Photovoltaic Applications, *ACS Nano 3 (2013) 2725.*
[28] R.C. Furneaux, W.C. Rigby, A.P. Davidson, The formation of controlled-porosity membranes from anodically oxidized aluminum, *Nature 337 (1989) 147.*
[29] G.E. Thompson, G.C. Wood, Porous anodic film formation on aluminum, *Nature 290 (1981) 230.*
[30] B. A. Scott, *Trans. Inst. Met. Finish. 43, (1965) 1.*
[31] G. C. Tu, I. T. Chen, K. Shimizu and Keikinzoku, *40, (1990) 382.*
[32] I.De Graeve, H. Terryn and G. Thompson, *J. Electrochem. Soc. 150(4), (2003) B 156.*
[33] I.De Graeve, H. Terryn and G. Thompson, *ATB Metall. 43, (2003) 34.*
[34] S. Ono, M. Saito and H. Asoh, *J. Electrochem. Solid-state Lett. 7, (2004) B21.*
[35] G. Patennarakis, and K. Moussoutzanis, *J. Corros. Sci. 43, (2001) 1433.*
[36] S. Z. Chu, K. Wada, S. Inoue, M. Isogai, Y. Katsuta, and A.Yasumori, *J. Electrochem. Soc. 153, (2006) B384.*
[37] P. Sheng Wei and T. Shih Shih, *J.Electrochem. Soc. 154, 11, (2007)C678-C683.*
[38] T. Aerts, I. De Graeve and H. Terryn, *J. Electrochim.Acta 54, (2008) 270-279.*